ORIGINAL ARTICLE

Adsorptive removal of toxic chromate and phosphate ions from polluted water using green-synthesized nanometal (Mn-Al–Fe) oxide

Sneha Latha Pala[1] · Wondwosen Kebede Biftu[1,2] · Suneetha Mekala[3] · Kunta Ravindhranath[1]

Abstract

Synthesizing nanomixed metal oxides via green routes and adopting them as adsorbents in water remediation methods is an important aspect of chemical research. In the present investigation, nanoparticles of mixed oxides of Mn-Al–Fe of size 6.19 nm are successfully synthesized adopting 'aloe vera gel' as capping agent and homogenous precipitation method for generating the precipitant (OH^-) by urea hydrolysis, in a viscous mother liquor of composition: 'glycerol:water (20:80)'. These nanoparticles are immobilized in Ca-alginate beads to prevent agglomeration. The mixed nanoparticles and beads are characterized and investigated for their sorption nature towards toxic chromate and phosphate ions. The adsorption mechanism is investigated by thermodynamic studies, isothermal and kinetic models. It is observed that chromate and phosphate can be simultaneously removed from waste water with the nanomixed metal oxides and beads at pH 7 and 10 respectively. The sorption capacities are 71.8 mg/g for phosphate and 87.3 mg/g for chromate with nanomixed metal oxides and 94.3 mg/g for phosphate and 109.8 mg/g for chromate with beads. The bead structure enhances sorption capacities besides permitting easy filtration. Thermodynamic studies confirm the endothermic and spontaneous nature of the adsorption. Pseudo 2nd-order kinetic models and Langmuir isotherms explain well the sorption mechanism. The adsorbents can be recycled for six cycles of re-generations and re-use. The sorbents developed are successfully applied for simultaneous remediation of chromate and phosphate from polluted water.

Keywords Nanomixed metal oxide · Beads · Aloe vera gel · Adsorption · Chromate and phosphate

1 Introduction

Green-synthesized nanomaterials are attracting researchers as adsorbents in developing water remediation methods [9, 12]. These bio-synthesized materials are proving to be effective adsorbents in water treatment in view of their high surface area and other surface characteristics inherited due to their nanosizes [60]. The endeavour of this investigation is

✉ Kunta Ravindhranath
   ravindhranath.kunta@gmail.com

1 Department of Chemistry, Koneru Lakshmaiah Education Foundation, Green Fields, Vaddeswaram-522 502, Guntur Dt, Andhra Pradesh, India

2 Ethiopian Radiation Protection Authority, Addis Ababa, Ethiopia

3 Department of Chemistry, RGUKT-Srikakulam, Andhra Pradesh, India

to develop effective nanobased adsorbents (green) to remove phosphate and chromate simultaneously.

Phosphate and chromate are potential toxicants present in industrial waste water. Water contamination with chromate arises mainly due to inadequately treated effluents from chromium-based industries while phosphate pollution is due to overutilization of fertilizers in agricultural activities, household uses, effluents from phosphate-based industries and erosion of phosphate rocks etc. [76]. The heavy metal chromium is a dangerous pollutant, because of its severe effects on human health [21]. Chromium consumption is linked to various diseases namely dermatitis, kidney and liver failures, ulceration, nerve tissues damage and even death [55]. Due to high solubility in water and strong oxidizing power, chromium (VI) is highly toxic to the aquatic environment [7]. Phosphate in water bodies causes 'eutrophication' and thereby causing reduction in the dissolved oxygen in water. The decrease in dissolved oxygen adversely

affects the aquatic life and loss of eco-cycles. In fact, recognizing phosphate contamination of water as a potential environmental threat, some countries passed legislations called 'phosphate acts' to prevent the usage of phosphate in detergents and other domestic utilities. The permissible limits by WHO are 0.05 mg/L for chromate (US Department of Health and Human Services 1991) [75] and 50 µg/L for phosphate (Bureau of Indian Standards, IS: 10,500–1991) [20]. Thus, the removal of chromate and phosphate is one of the environmental concerns.

Several methods based on ion exchange, membrane filtration, chemical precipitation, electrodialysis, adsorption etc., have been employed to remove phosphate or chromate from waste water (Mohammad et al., 2014 [51]; [6, 7, 19, 62, 65, 66]. These methods are non-economical, are not applicable to treat large quantities of water and, moreover, need constant expert supervision. Adsorption methods are preferred methods because of their low-operational cost, being environmentally friendly and high efficiency [67].

Adopting non-conventional materials and bio-materials as adsorbents is a recent trend in this aspect of water remediation. Various adsorbents such as marble dust, volcanic ash and sand [28, 29], bio-chars derived from crop straws [37], egg shells [22], modified wheat straw [58], marble waste [17], corn stalks (Fan et al., [31], magnetic coal [33], activated carbon (AC) and sand/zeolite mixture (S/Z) [45, 48], AC from stems of *Carissa carandas* plant [13] and AC from leaves of Magnoliaceae plant [14] have been investigated for the removal of phosphate or chromate from waste water.

Nanobased adsorbents are also employed to enhance the sorption capacity of adsorbents for phosphate or chromate. The sorbents investigated are as follows: iron-magnesium nanocomposite (nFe^0-Mg) [46], nanoscale zero-valent iron (Fe^0) coated with different layered hydroxide coatings (Mg/Al/Ca $(OH)_n$) [47], nanoscale zero-valent iron (nZVI), PAA-nZVI, PVP-nZVI, CMC-nZVI and PSM-nZVI [30], *Phyllostachyspubescens* biomass–loaded Cu–S nanospheres [1], zirconia-coated magnetite nanoparticles [77, 79], nanoscale zero-valent iron (nZVI) [4], bimetallic nanoscale zero-valent iron (Fe^0/Cu) and foamed nickel-based La $(OH)_3$ nanowire [82].

These investigations are devoted to remove either phosphate or chromate and not both at a time. Furthermore, many of these adsorbents suffer from either low adsorption capacity or high cost or poor regeneration. Effective adsorbents for the simultaneous removal of phosphate and chromate from polluted water are less reported. The present investigation is an attempt in this direction employing nanocrystallites of 'trinary mixed metal (Mn-Al–Fe) oxides' with or without doping in Ca-alginate beads as adsorbent.

In this investigation, the manganese-based nanotrinary mixed metal (Mn-Al-Fe) oxides are synthesized via new green routes. Such particles are expected to be bio-compactable with improved sorption nature because the capping or stabilizing agents employed are from natural sources. Investigations in identifying the effective stabilizing and/or capping agents from plant sources in place of conventional toxic agents is one of interesting research aspects (Biftu and Ravindhranath, [10]. In the present investigation, 'aloe vera gel' is identified to have good capping and/or stabilizing nature. This bio-extract coupled with the slow generation of precipitant (OH^-) (urea hydrolysis—homogenous methods) from the viscous mother liquor of composition, glycerol + water (20:80), has resulted in the successful synthesis of uniform-sized nanocrystallites of mixed metal (Mn-Al–Fe) oxides. The particles have been observed to have good adsorptivities for toxic 'phosphate and chromate' at the neutral pH 7. Agglomeration of nanoparticles and slow filtration are the main limitation of using nanoparticles as adsorbents. Hence, to overcome these disadvantage, the mixed nanoparticles have been immobilized by cross-linking Na-alginate with Ca^{2+} ions, resulting in beads (Biftu and Ravindhranath, [11]. Thus, obtained beads have been observed in this investigation to have enhanced adsorptivities for 'phosphate and chromate' at pH 10. The good adsorptivities of nanomixed metal oxides and their beads for 'phosphate and chromate' at pH 7 and pH 10, respectively, enable us to pursue the concept of the simultaneous adsorption of these pollutants from waste water.

Hence, in the present study, mixed nanocrystallites of metal (Mn-Al–Fe) oxide are synthesized via new green methods. These particles are immobilized in calcium alginate beads. The nanomaterial and beads are characterized and their sorption capacities are investigated with respect to various parameters for the simultaneous removal of 'phosphate and chromate'. The sorption mechanism is analysed by thermodynamic studies, isothermal and kinetic models. The developed procedures are applied to treat real water samples.

2 Materials and method

2.1 Chemicals and solutions

All chemicals and reagents used throughout this research work were of A.R. grade. The chemicals $Al_2(SO_4)_3$, $MnSO_4$.H_2O, $NH_4Fe(SO_4)_2$.$12H_2O$, $K_2Cr_2O_7$, KH_2PO_4, Conc. HCl, NaOH, NH_3 and $CaCl_2$ were procured from Merck, India Pvt. Ltd. and S.D. Chemicals, India. Solutions were prepared as described in the literature [3, 64]. The simulated stock solutions of 'phosphate and chromate' were prepared using distilled water.

2.2 Synthesis of mixed nanocrystallites of oxides of Mn, Al and Fe

The aloe vera gel was scrapped from the plant, stirred to obtain a homogeneous solution and stored in a refrigerator at 5 °C. This gel served the purpose of a capping agent.

Individual nano-MnO$_2$, Al$_2$O$_3$ and Fe$_3$O$_4$ 2.0 g each of A.R. MnSO$_4$.H$_2$O, Al$_2$ (SO$_4$)$_3$ or NH$_4$ Fe(SO$_4$)$_2$.12H$_2$O were dissolved in 100 mL of 'water:glycerol (80:20)' blend having 1.0 mL of Conc. HCl. Then, 1.5 g of aloe vera gel was added and stirred to a homogenous solution. Glycerol content in the solution increases the viscosity of the media. Then, 5.0 g of urea in small portions (not at a time) was added to the solution while the solution was under slow heating and gradually raising the temperature to 85 °C. Urea undergoes hydrolysis with the rise of temperature, resulting in the generation of ammonia which in turn raises the pH of the solution. The heating was stopped when the solution attains pH 9, but stirring was continued for a further 3 h. Under the conditions of low viscosity of mother liquor, slow generation of the precipitant and the capping ability of aloe vera gel, nanosized crystallites of metal oxides were successfully synthesized. The particles were separated by centrifugation and washed

with distilled water. Then, the particles were dried at 105 °C and calcinated at 550 °C for 3 h in a muffle furnace.

Mixed oxide nanocrystallites The procedure adopted was similar to that of the synthesis of individual oxides but with the dissolution of a mixture of 2.0 g of each salt (MnSO$_4$.H$_2$O, Al$_2$(SO$_4$)$_3$ and NH$_4$Fe (SO$_4$)$_2$.12H$_2$O) in the mother liquor (glycerol:water: 20:80). The mixed nanooxide crystallites were named as n(Mn-Al–Fe) oxide and preserved in an air-tight bottle. The crystallite size was determined by XRD analysis (Fig. 2 and Table S1).

Calcium alginate beads doped with mixed nanooxides 2.5 g of sodium alginate in 100 mL of distilled water was heated (70 °C) with stirring to a gel-like solution. Then, 2.0 g of mixed nanometal oxide was added and stirring was continued for 1 h, to obtain a homogeneous dispersed metal oxide solution. Thus, the resulting solution was cooled to room temperature and added drop-by-drop into a previously cooled 3.0% CaCl$_2$ (10 °C) solution with the aid of a dropper. Beads impregnated with 'nanoparticles' were formed as depicted in Fig. 1. Thus, formed beads were digested for 12 h with its mother liquor. Beads were filtered, washed and dried at 75 °C for 1 h. The beads were named as follows:
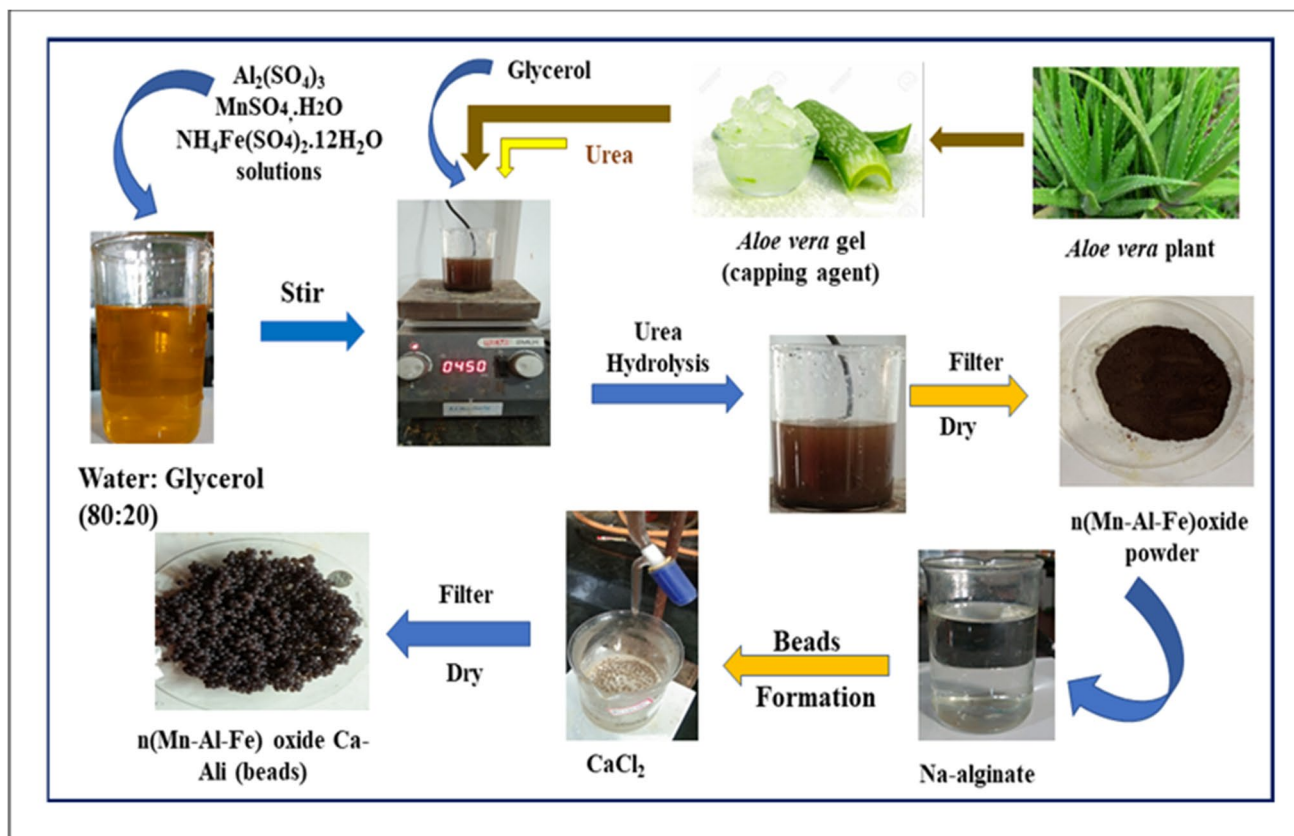

Fig. 1 Various phases of syntheses of adsorbents

n(Mn-Al–Fe) oxide-Ca-Ali (beads). Various stages of the synthesis of beads are presented in Fig. 1.

Adsorption experiments Batch adsorption processes were adopted [74]. Simulated individual solutions of phosphate and chromate were used for investigating the effect of various parameters on the adsorption of phosphate and chromate. Then simulated admixtures of phosphate and chromate were treated at the conditions established during the course of this investigation for individual ions to assess their applicability.

2.2.1 Optimization of adsorption conditions

Known amounts of mixed nanometal oxide and beads, ranging from 0.01 to 0.08 g/150 mL, were added to simulated phosphate (25.0 mg/L) or chromate (20.0 mg/L) solutions. The initial pH of the solutions was adjusted between 2 and 12. The solutions were agitated for needed times ranging from 10 to 100 min at 350 rpm in an orbital shaker. The sorbents were filtered. The filtrate was analysed for the residual phosphate or chromate content spectrophotometrically using Molybdenum Blue method for phosphate and Diphenyl Carbazide method for chromate (APHA, Standard Methods, [3]). For assessing the effect of one parameter on the adsorptivity of the sorbent, the targeted parameter was varied while all other parameters were maintained constant. After optimizing the pH, sorbent concentration and time of contact, the effect of the initial concentration of phosphate or chromate on the percentage of adsorption was investigated by varying the initial concentrations from 10 to 60 mg/L. Similarly, the effect of temperature on the adsorptivities of the sorbents was studied by varying the temperature from 303 to 333 K. Percentage removal of chromate or phosphate and sorption capacities of adsorbents were evaluated [13]. Findings are presented in Figs. 6 and 7. The optimum conditions of adsorption for both the ions at room temperature of 303 K with mixed nanooxide as adsorbent were found to be as follows: pH: 7, sorbent dosage: 0.055 g/150 mL; equilibration time: 40 min. In the case of beads, the optimum conditions were as follows: pH: 10; sorbent dosage: 0.05 g/150 mL; and equilibration time: 60 min at room temp (303 K).

2.2.2 Mixtures of simulated phosphate and chromate solutions

With mixed oxide, both the adsorbates were shown maximum adsorptiviies at pH 7 while with beads at pH 10. Hence, at these pH values, simulated mixed solutions of 'chromate and phosphate' were investigated to assess whether the optimum conditions arrived in the case of individual ions also 'hold good' for the mixtures of the adsorbates. In Table 2, results were presented. Except adsorbent dosage and time of equilibration, the rest of the parameters remain constant for the simultaneous removal of 'phosphate and chromate'. The optimum dosage is 0.13 g/150 mL for nanomixed oxides and 0.11 g/150 mL for beads. The optimum contact time is 60 min for nano-mixed metal oxide and 90 min for beads.

2.3 Characterization of adsorbents

The mixed nanometal oxides and beads were characterized for conventional properties by adopting the procedures as described in the literature [14],BIS: Bureau of Indian Standards., [15]; ASTM D4607-94., [5] (Table 1). Further using XRD, FTIR, FESEM and EDX techniques, the sorption surface nature was assessed. Figures 2 to 5 comprise of the results of these studies.

2.4 Applications

Effluent samples from industries based on phosphate and chromate and also polluted lake waters from Guntur District of Andhra Pradesh were collected and analysed for the actual content of phosphate and chromate. Then, these samples were subjected to the treatment with the sorbents developed in this investigation.

Table 1 Physico-chemical properties of nanometal oxide and beads

S. no	Parameter	Adsorbent			
		n(Mn-Al–Fe) oxide		n(Mn-Al–Fe) oxide-Ca-Ali (beads)	
1	Apparent density (g/mL)	0.36		0.32	
2	Moisture content (%)	3.21		2.09	
3	Iodine number (mg/g)	680		620	
4	Particle size (μ)	6.19		9.7	
5	Crystallinity %	82.45		45.6	
6	BET analysis-surface area (m²/g)	Before	After	Before	After
		304.23	Chromate: 201.00 Phosphate: 192.34	328.60	Chromate: 214.47 Phosphate: 218.56

Fig. 2 XRD analysis of **a** nAl$_2$O$_3$; **b** nFe$_3$O$_4$; **c** nMnO$_2$; **d** (Mn-Al–Fe) oxide; and **e** n MnO$_2$ -Al$_2$O$_3$-Fe$_3$O$_4$-Ca-Ali (beads)
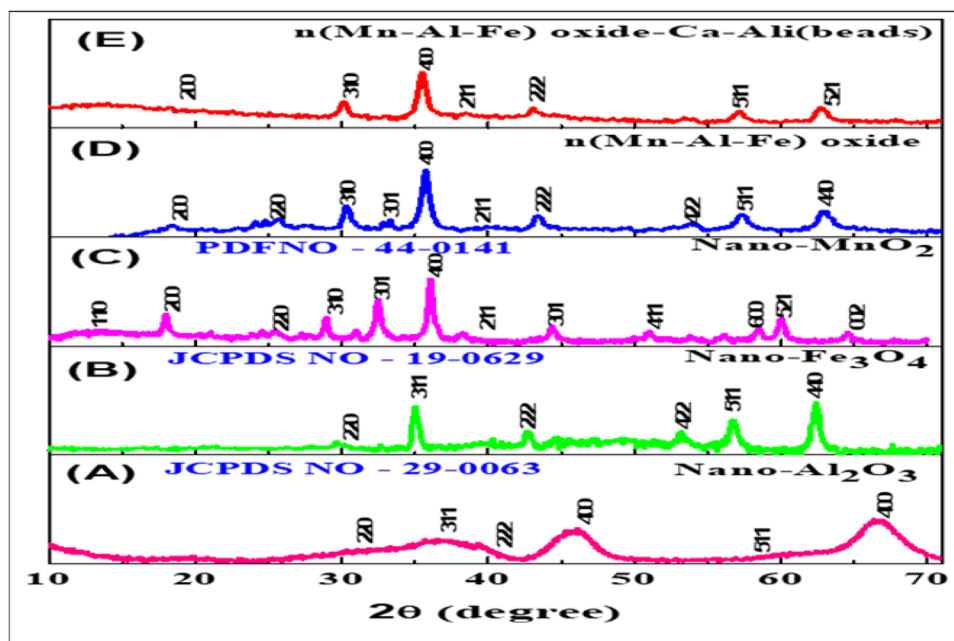
3 Results and discussion

3.1 Characterization studies

3.1.1 Physicochemical parameters

Moisture content, apparent density and ash content of sorbents were assessed adopting standard methods [14], iodine number [15] and particle size (ASTM D4607-94 [5]). Adsorbent surface areas 'before and after adsorption' of phosphate and chromate were estimated using BET analysis [27]. Table 1 depicts the results. The reductions in the surface area of sorbents after sorption of adsorbates emphatically confirm the sorption.

3.1.2 XRD analysis

In Fig. 2a to e, XRD spectra of nanoparticles of nMnO$_2$, nAl$_2$O$_3$, nFe$_3$O$_4$, mixed metal (Mn-Al–Fe) oxides and beads were presented. Nano-Al$_2$O$_3$ shows diffraction peaks at 2θ = 32.3°, 36.01°, 39.5°, 45.8°, 62.6° and 66.6° (Fig. 2a) and they may be attributed to the planes of (220), (311), (222), (400), (511) and (400) of a pure cubic structure of γ-Al$_2$O$_3$ as per JCPDS card no 29–0063. Nano-Fe$_3$O$_4$ displayed a series of peaks at 2θ = 29.6°, 35.1°, 42.6°, 53.4°, 56.9° and 62.6° pertaining to the planes (220), (311), (222), (422), (511) and (440) (Fig. 2b), as per JCPDS card no 19–0629. Nano-MnO$_2$ (Fig. 2c) shows peaks at 12.7°, 18.0°, 25.4°, 29.0°, 36.01°, 38.1°, 44.3°, 50.8°, 55.8°, 60.0° and 64.5° and they can be assigned to the planes (110), (200), (220), (310), (400), (211), (301), (411), (600), (521) and

(002) respectively of cubic structure as per PDF card no. 44–0141.

Nanomixed metal (Mn-Al–Fe) particles have exhibited peaks at 2θ = 18.0°, 25.4°, 29.0°, 33.6°, 36.1°, 38.1°, 42.6°, 44.3°, 50.8°, 54.3°, 57.8°, 60.0° and 64.5° (Fig. 2d). Comparing these diffraction peaks with the individual peaks of nAl$_2$O$_3$, nMnO$_2$ and nFe$_3$O$_4$, it may be inferred that many peaks pertaining to individual oxides have appeared in the mixed oxides with slight variation in the peak positions and intensities. This indicates the formation of mixed crystals of metal (Mn-Al–Fe) oxides of nanosize. The crystallite size of the individual metal oxides and their mixed oxides were evaluated as per Scherrer equation, $L = \frac{k\lambda}{B\cos\theta}$. The results are presented in Table S1. The particle crystalline sizes were found to be 25.9 nm for MnO$_2$; 12.9 nm for Al$_2$O$_3$; 11.16 nm for Fe$_3$O$_4$; and 6.19 nm for metal oxides [18],Dorofeev, [24]; [1].

Ca-alginate beads doped with nanometal oxides shows prominent peaks at 2θ = 25.4°, 29.1°, 36.1°, 38.4°, 42.6°, 56.5° and 60.0° (Fig. 2e). In comparison of these spectral features with the mixed oxides, it may be noted that some peaks are missing and some other peaks have changes in their intensities, and even broadening of the peaks was also observed. This indicates the partial loss of crystallinity (semi-crystalline) due to the formation of beads. The similar observations were reported in the case of iron-magnesium nanocomposite (nFe^0-Mg) compared to nanoscale zero-valent iron (nFe^0) [46] and in the case of C-Fe^0 [Mg/Fe] compared to C-Fe^0 [Al/Fe] and C-Fe^0 [Ca/Fe] particles [47]. This is a favourable condition for the adsorption process to take place and it endows conducive adsorption nature for the beads.

3.1.3 FTIR analysis

Spectra observed before and after sorption of phosphates and chromate by the sorbents are presented in Fig. 3a and b.

Observations with nanomaterials (Fig. 3a) Various spectral peaks were noted. Broad peaks of different shapes with maxima at 3152 cm^{-1} pertaining to '-OH stretching' were observed both in the spectrum taken 'before and after' adsorption [61]. The 'Fe-OH' stretching peak at 1606 cm^{-1} (before adsorption) [39, 81] was shifted to 1625 cm^{-1} and 1618 cm^{-1} with varying intensities after adsorption of phosphate and chromate respectively. Mn/Al–OH stretching peak at 1142 cm^{-1} (before spectrum) [42] was shifted to 1003 and 1073 cm^{-1} (phosphate) and 1118 cm^{-1} (chromate) with marked changes in their intensities after adsorption, indicating the formation of Mn/Al-O-PO_4^{3-}/CrO_4^- [42].

New peaks at 951 cm^{-1} for phosphate and 974 cm^{-1} for chromate pertaining to Al/Mn–O stretchings [16] were observed in the after-adsorption spectrum. The intensive peak at 826 cm^{-1} pertains to 'O-Mn/Fe–O' bending [68] in the before adsorption spectrum was almost disappeared with little peaks at 816 cm^{-1} (phosphate) and 810 cm^{-1} (chromate) after adsorption. Two small peaks, one at 777 cm^{-1} after phosphate adsorption and the other at 774 cm^{-1} after chromate adsorption, have appeared in the after-adsorption spectrum and may be due to the bending vibrations of Al-O-CrO_4^-/PO_4^{3-} [42]. The vibrational peak at 705 cm^{-1} due to 'Al–O–Al' stretching [83] has been shifted to 725 cm^{-1} with enhanced intensities after phosphate and chromate sorption. The peak at 653 cm^{-1} (before adsorption) has completely disappeared after adsorption of phosphate and chromate. The peak at 623 cm^{-1} of Fe/Mn–O (before adsorption) [57] has been shifted to 620 cm^{-1} and 613 cm^{-1} after adsorption of phosphate and chromate respectively.

The new sharp frequencies appeared at 655 cm^{-1} and 661 cm^{-1} after adsorption of phosphate and chromate, which may be due to the asymmetric stretching of 'Mn-PO_4^{3-}/CrO_4' [25, 42]. A sharp small peak at 618 cm^{-1} before

Fig. 3 FTIR spectra: **a** nanomixed metal oxides; **b** Ca-alginate beads doped with nanomixed metal oxides before and after adsorption of phosphate and chromate
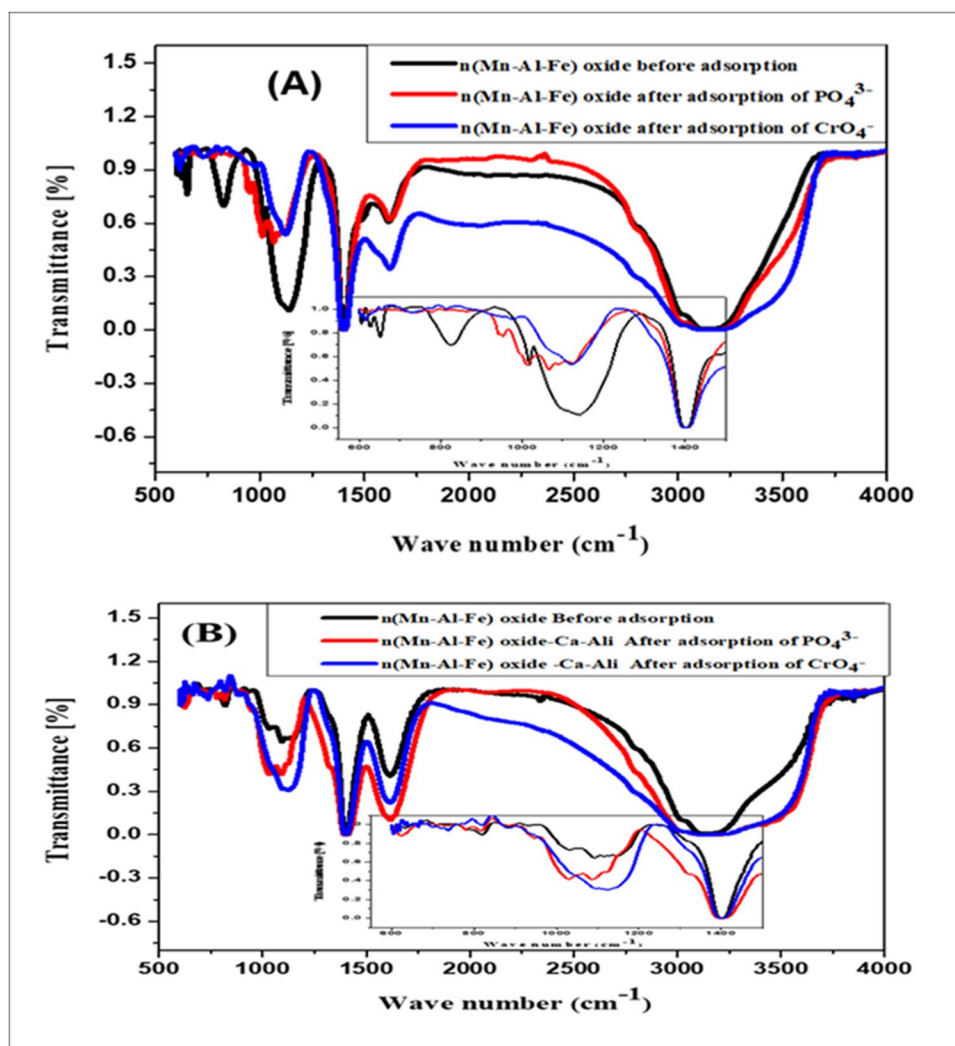
adsorption was shifted to 620 and 623 cm^{-1} after adsorption of phosphate and chromate respectively. It may be due to asymmetric stretching of 'Mn/Al-PO$_4$$^{3-}$'. Sharp frequency due to 'Fe/Mn–O' vibrations at 603 cm^{-1} [81] appeared before adsorption was shifted to 597 cm^{-1} and 600 cm^{-1} after phosphate and chromate adsorption respectively, resulting in the formation of Fe/Mn–O-PO$_4$$^{3-}$/CrO$_4$$^-$ [61, 78].

Observations with beads (Fig. 3b) The spectra of beads show additional peaks relating to 'O=C-O-' at 1607 cm^{-1}, '-C-O-' at 1111 cm^{-1} and strong broad peak from 3093 to 3239 cm^{-1} for -OH stretchings. After phosphate adsorption, dual peaks of almost equal intensities have appeared at 1015 cm^{-1} and 1081 cm^{-1} while in the spectrum of chromate adsorption, an intensive single peak appeared at 1108 cm^{-1}, indicating a sort of complex formation between the adsorbent and phosphate/chromate. After adsorption of phosphate or chromate, the broad peak of –OH stretchings between 3067 and 3234 cm^{-1} (before spectrum) with maxima at 3147 cm^{-1} has been further broadening after the adsorption of phosphate and chromate. The ester (O=C-O) peak stretching at 1607 cm^{-1} (in the before spectrum) has been shifted to 1621 and 1614 cm^{-1} with high variations in the intensities after the adsorption of phosphate and chromate respectively.

The frequency of Al/Mn–O stretchings at 929 cm^{-1} (before spectrum) has been shifted to 945 cm^{-1} after adsorption of phosphate but the peak completely vanished after adsorption of chromate. The vibrational peak at 735 cm^{-1} due to 'Al–O–Al' bending has been shifted to 737 cm^{-1} after adsorption of chromate and completely vanished after the adsorption of phosphate. Additional bands with varying intensities have appeared at 606, 616, 649, 652, 664, 676 and 699 cm^{-1} after the adsorption of chromate. The peak

pertaining to asymmetric stretchings of 'Mn/Al-PO$_4$$^{3-}$' at 630 cm^{-1} was shifted to 623 and 631 cm^{-1} with varying intensities after adsorption of phosphate and chromate respectively.

Thus, the change of spectral characteristics between 'before' and 'after' adsorption of phosphate and chromate strongly suggests the adsorption of the latter 'onto' the nanocomposite and beads.

3.1.4 FESEM and EDX spectral analysis

Clearly visible agglomerated nanoparticles are noticed in FESEM images of nanocomposite taken before adsorption of phosphate and chromate (Fig. 4a). Voids, boundaries and edges were noticed. These features partially or completely have disappeared in the spectrum after adsorption, yielding to a smooth surface (Fig. 4b).

In the case of beads, there is a drastic contrast between the images taken before and after the adsorption of phosphate and chromate. The plasticized aggregates of particles with pores were noticed in beads (Fig. 4c). The pores, voids, boundaries and edges are disappeared after adsorption of chromate phosphate and chromate (Fig. 4d). These changes in the surface morphologies confirm the occurrence of sorption.

Further evidence of adsorption was noted in EDX spectra. Peaks pertaining to Mn, Al, Fe and O were presented in before spectra of nanocomposite (Fig. 5a). In addition to these peaks, peaks related to P and Cr were noticed in the elemental spectra taken after adsorption of phosphate and chromate (Fig. 5b). Similarly, the bead spectrum has Mn, Al, Fe, Ca, C and O peaks (Fig. 5c). After adsorption, Cr and P peaks appeared (Fig. 5d). The presence of Cr and P peaks after adsorption indicates the adsorption of chromate and phosphate by the two adsorbents (Table 2).

Fig. 4 SEM images: n(Mn-Al–Fe) oxide: **a** before and **b** after phosphate and chromate adsorption; n(Mn-Al–Fe) oxide-Ca-Ali (beads): **c** before and **d** after phosphate and chromate adsorption
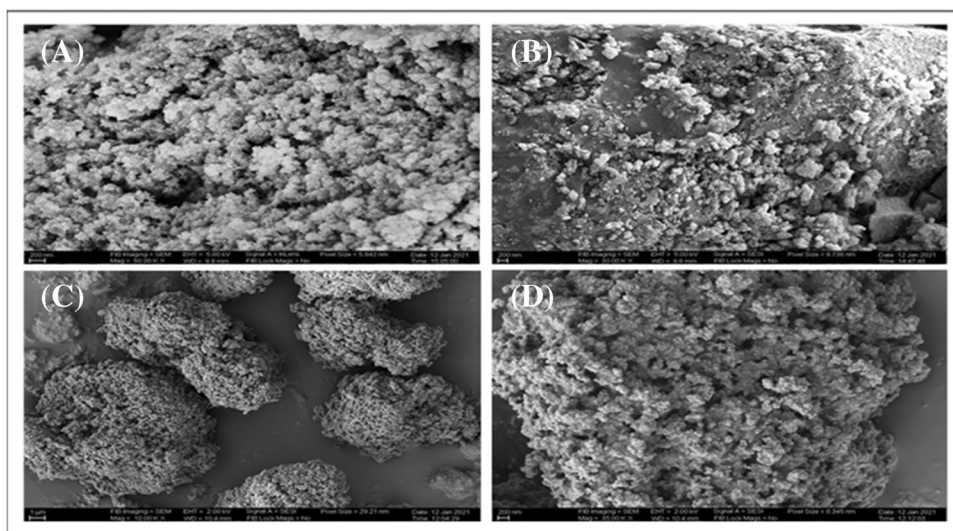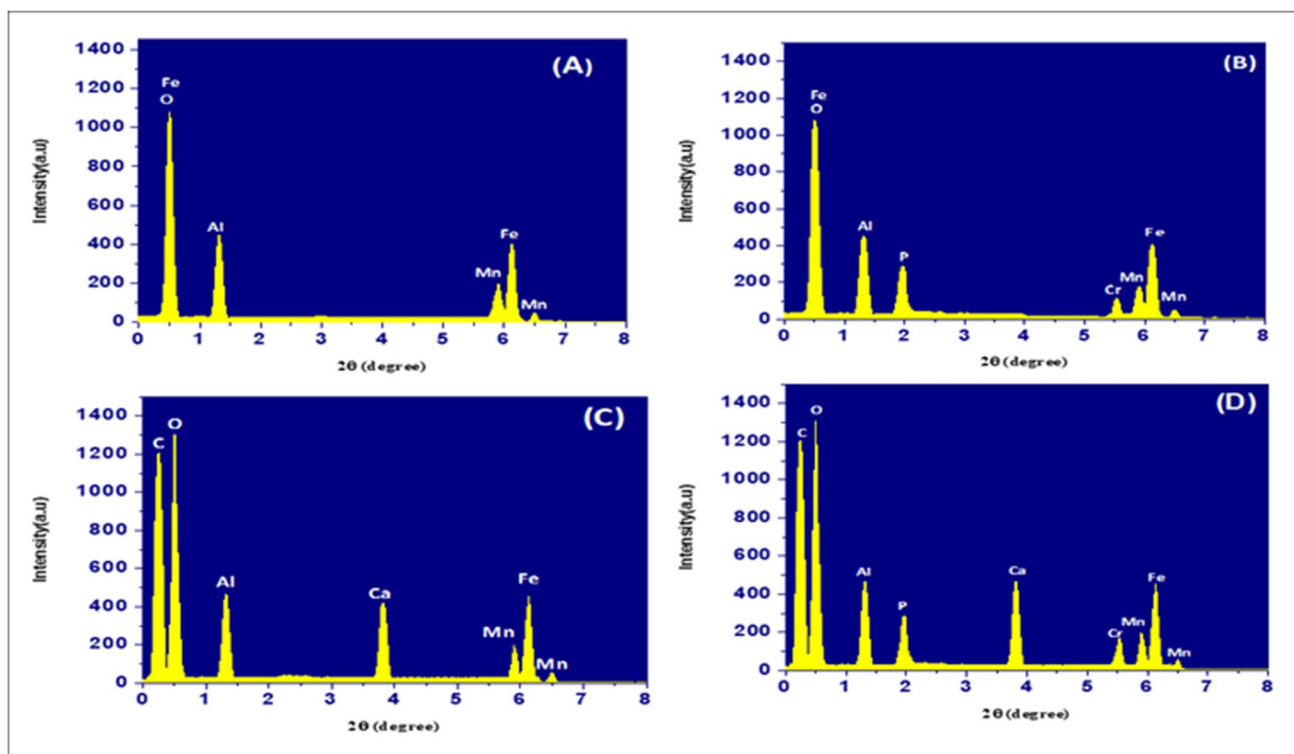
Fig. 5 EDX spectrum of nanomixed oxides: **a** before adsorption and **b** after adsorption; beads: **c** before adsorption and **d** after adsorption

Table 2 Simultaneous removal of chromate and phosphate from simulate water*

Samples	Concentration of mixture Chromate + phosphate (mg/L)		After adsorption mg/L		% removal	

A: Nanocomposite: n(Mn-Al–Fe) oxide optimum conditions: pH: 7; dosage of composite: 0.13 g/150 mL; contact time: 60 min; rpm: 350; temp.: 30 ± 1 °C)

	Cr (VI)	Phosphate	Cr(VI)	Phosphate	Cr(VI)	Phosphate
1	4.5	4.5	0	0	100	100
2	7.5	9.5	0	0	100	100
3	9.5	15.5	0	0	100	100
4	12.0	20.0	0.05	0.27	99.5	98.6
5	16.0	24.0	0.61	1.08	96.2	95.5

B: n(Mn-Al–Fe) oxide-Ca-Ali (beads): optimum conditions: pH: 10; dosage of composite: 0.11 g/150 mL; contact time: 90 min; rpm: 350; temp.: 30 ± 1 °C)

1	4.5	4.5	0	0	100	100
2	7.5	9.5	0	0	100	100
3	9.5	15.5	0	0	100	100
4	12.0	20.0	0	0.19	100	99.0
5	16.0	24.0	0.34	1.02	97.8	95.7

*The values are average of five estimations; S.D: ± 0.18

3.2 Factors influencing the absorptivity

Solution pH markedly affected the adsorption of adsorbates (Fig. 6a). For nanocomposite, the optimum pH was 7 and for beads 10. Below and above these pHs, the % removal was decreased for both the adsorbates. The pHzpc = 7.2 for nanocomposite and 7.6 for beads (Fig. 6b). At these pH values, the surface of the adsorbent is neutral. Above these values, the surface is charged negatively due to the dissociation of the functional groups, and below, the surface acquires a positive charge due to protonation of the functional group such as -OH. Interestingly, maximum adsorption was noticed
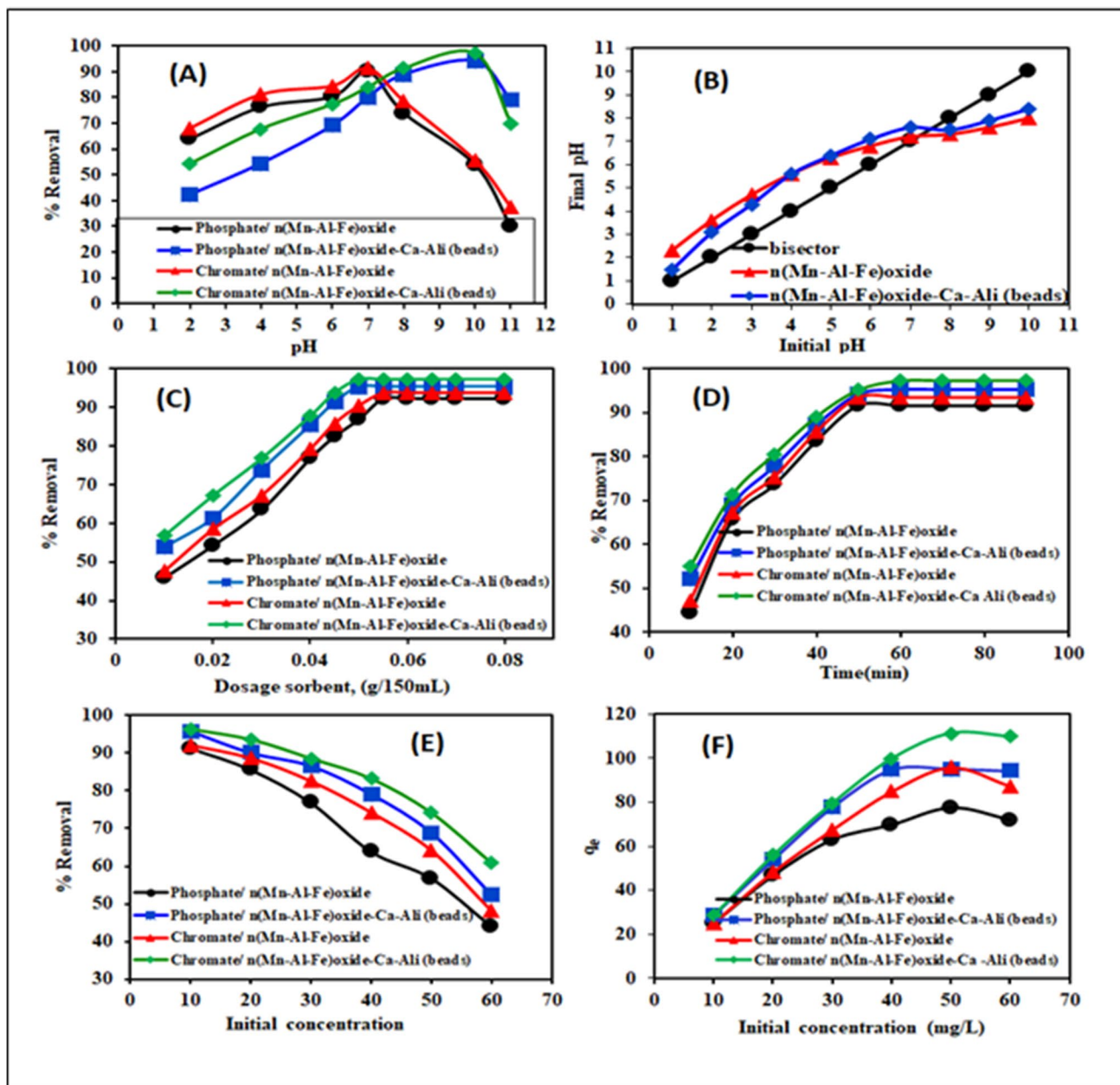
Fig. 6 **a** Effect of pH; **b** pHzpc evaluation; **c** effect of dosage; **d** effect of contact time; **e** effect of initial concentrations; and **f** adsorption capacities, q_e vs initial concentration

at 7 and 10 though the predominant species at these pH values are negatively charged i.e., $H_2PO_4^-$ and $HCrO_4^{2-}$. At these pH values, the surfaces of nanocomposite and beads are neutral or negatively charged. Hence, the interaction between the functional groups of adsorbent and adsorbate is not mere electro-statical interactions but involves a sort of complex formation between the functional groups of the adsorbents and phosphate/chromate. This is supported by high ΔH values for phosphate and chromate: 63.83 J/mol and 66.10 J/mol for nanocomposite and 55.88 J/mol,

53.89 J/mol for beads respectively (Table 3). Further confirmation can be inferred from the presence of spectral peaks of $Fe–O-PO_4^{3-}/CrO_4^{2-}$, $Mn-PO_4^{3-}/CrO_4^{2-}$ and $Al-O-CrO_4^{2-}/PO_4^{3-}$ etc. in the FTIR spectrum taken after adsorption of phosphate and chromate.

The optimum dosages needed for the maximum adsorption of phosphate and chromate were investigated (Fig. 6c) and found to be 0.055 g/150 mL for composite and 0.05 g/150 mL for beads. At low concentrations of dosage, the adsorption was linearly increased with a progressive

Table 3 Evaluated thermodynamic parameters

| Adsorbate	ΔH (kJ/mol)	ΔS (J/mol)	ΔG (kJ/mol)				R^2
			303°K	313°K	323°K	333°K	
A: Nanocomposite [n(Mn-Al–Fe) oxide]							
Phosphate	63.83	384.6	− 52.69	− 56.54	− 60.38	− 64.23	0.92
Chromate	66.10	394.6	− 53.46	− 57.4	− 61.35	− 65.3	0.98
B: Beads [n(Mn-Al–Fe) oxide-Ca-Ali]							
Phosphate	55.88	367.6	− 55.49	− 59.17	− 62.84	− 66.52	0.97
Chromate	53.89	363.7	− 56.3	− 59.94	− 63.58	− 67.21	0.97

increase in dosage, but after the optimum dosages, a kind of steady state was reached. At low dosages adsorbent, the increase in adsorptivity may be due to the increase in the availability of active sites with an increase in sorbent concentration. The steady state at higher dosages may be due to the overcrowding of the adsorbent particles leading to overlapping and/or blocking of the surface-active sites [12].

Time of contact between sorbents and adsorbates was investigated and the findings are presented in Fig. 6d. The adsorption of phosphate and chromate was rapid and linear initially and attained a kind of steady state after 40 min for metal nanomixed oxide and 60 min for beads. The initial rapid adsorption was due to the availability of sufficient surface-active sites per ion of adsorbate. But active sites were limited as the adsorbent dosages was fixed. With the progress of time, the active sites were increasingly used up i.e. availability of active sites per ion decreased, resulting in a decrease in % removal [17, 56]. When all the active sites on the adsorbent surface were exhausted with time by phosphate and chromate ions, a steady state was resulted [12, 63].

Initial concentrations of adsorbates markedly affected the adsorption of phosphate and chromate (Fig. 6e and f). With an increase in the initial concentration of 'phosphate or chromate', the % of adsorption was decreased. But it was interesting to note that adsorption capacities of adsorbents were increased as the initial concentration of phosphate

and chromate was increased. In fact, the adsorption capacities (q_e) were increased for nanocomposite from 24.9 to 71.8 mg/g (for phosphate) and from 25.1 to 87.3 mg/g (for chromate) and for beads from 28.7 to 94.3 mg/g (for phosphate) and from 28.8 mg/g to 109.0 mg/g (for chromate). As the adsorbate concentration was increased, the active sites needed for sorption process to occur were more. With the increase in the initial concentration of the adsorbate, the concentration gradient between the concentrations of adsorbates in bulk of the solution with their concentrations on the surface of the adsorbents also increased. This caused more diffusion of adsorbate ions towards the surface of the adsorbents, resulting in high adsorptivities, q_e (Biftu and Kunta, [54]).

The effect of temperature on the adsorption of phosphate and chromate was investigated by varying the temperature from 303 to 333 K (Fig. 7a). For nanocomposite as adsorbent, the percentage removal was increased from 45.2 to 89.8 (q_e: 24.9 to 71.8 mg/g) for phosphate and 50.3 to 91.5 (q_e: 25.1 to 87.3 mg/g) for chromate. In the case of beads, percentage removal was enhanced from 69.5 to 94.6 (q_e: 28.7 to 94.3 mg/g) for phosphate and 75.6 to 95.7 (q_e: 28.8 to 109.8 mg/g) for chromate. Adsorbate ions acquire more movement with the increase of solution temperature and also the surface of the adsorbent is more open for allowing the penetration of the adsorbate ions deeper into the matrix of

Fig. 7 **a** Effect of temperature; **b** Van't Hoff plot
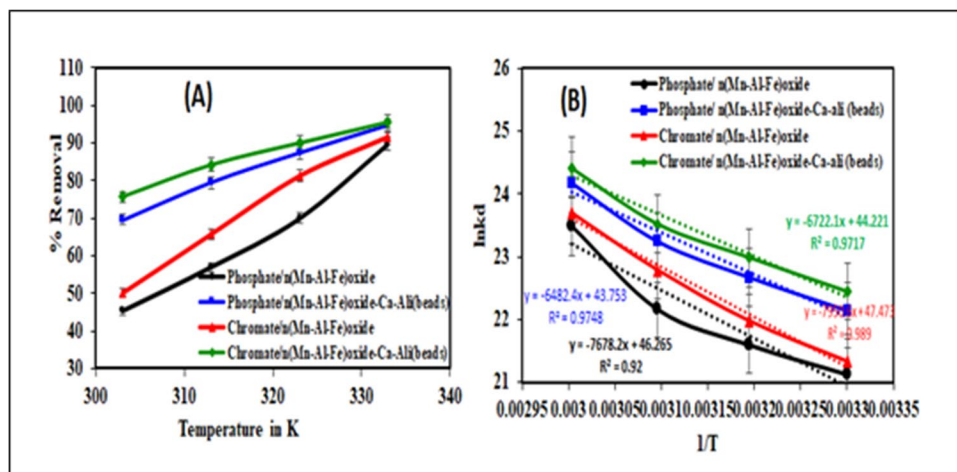
the adsorbents, resulting in more adsorption with an increase of temperature [2, 71].

Co-ions effect The presence of twofold excess of common anions, Cl^-, F^-, SO_4^{2-}, NO_3^- and HCO_3^-, was investigated with simulated solutions of phosphate and chromate (Fig. 8). These ions marginally effected the adsorption of phosphate and chromate. Fluoride interfered to some extent. The co-anions compete with phosphate/chromate for the active sites of the adsorbents. Size of ions, columbic repulsions, polarizability, electronegativity, magnitude of charge etc. affect the extent of interference [17, 38]. Fluoride in view of its small size and highest electronegativity competes more with adsorbate anions, causing interference.

3.3 Simultaneous phosphate and chromate adsorption

To assess whether the extraction conditions established with individual phosphate and chromate hold good for their simultaneous extraction, investigations were undertaken with synthetic simulated mixed solutions of phosphate and chromate of different compositions. The solutions were subjected to the adsorption using the two adsorbents at the optimum conditions arrived for individual phosphate and chromate. The optimum conditions observed for individual pollutants (chromate/phosphate) at room temperature of 303 K are as follows: pH: 7; sorbent dosage: 0.055 g/150 mL; and equilibration time: 40 min for nanometal oxides as adsorbent; and pH: 10, sorbent dosage: 0.05 g/150 mL; and equilibration time: 60 min for beads.

It was observed that for simultaneous removal of phosphate and chromate, enhanced sorbent dosages and time of equilibriums were needed as depicted in Table 2. For nanocomposite, the time of equilibration was to be increased from 40 to 60 min and for beads from 60 to 90 min. Furthermore, the sorbent dosage was to be enhanced from 0.055 to 0.13 g/150 mL for nanocomposite and 0.05 to 0.11 g/150 mL for beads. The other conditions of adsorption remain the same as that of individual adsorbates (Table 2). From the table, it can be inferred that the effective simultaneous removal of and phosphate and chromate is possible.

3.4 Thermodynamic studies

Thermodynamic parameters namely Gibbs free energy, entropy and enthalpy were evaluated using equations: $\Delta G = \Delta H - T\Delta S; \Delta G = -RtlnK_d$; and $lnK_d = \frac{\Delta S}{R} - \frac{\Delta H}{RT}$ [69, 70]. The sign and magnitude indicate the nature of adsorption of phosphate and chromate (Fig. 7b) and the values are presented in Table 3.

The negative values of ΔG indicate the spontaneous adsorption of and phosphate and chromate 'onto' the adsorbents. More negative values at enhanced temperatures are indicative of the favourable nature of the sorption process as the temperature is increased. Positive ΔH values are indicative of the endothermic nature of the sorption process. Furthermore, the high values for phosphate, 63.83 J/mol (nanocomposite) and 55.88 J/mol (beads), and for chromate, 66.10 J/mole (nanocomposite) and 53.89 J/mol (beads), strongly suggest that the adsorption mechanism is via some sort of complex formation between phosphate/chromate with the functional groups of the adsorbents. The positive values of ΔS and their magnitude indicate the degree of disorder existing at sorbent/solution interface. As the degree of disorder is more, the chances of adsorbate ions to cross over the interface are more, and hence, high adsorption.

Fig. 8 Interference of Co-anions on the adsorption
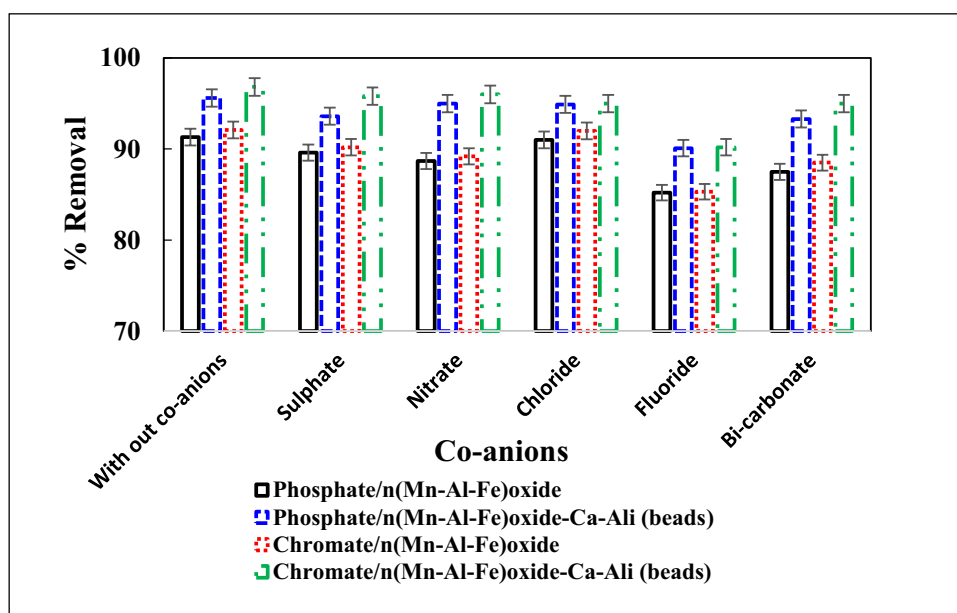
3.5 Adsorption isotherms

The nature of adsorption of phosphate and chromate 'onto' the adsorbents was analysed by four isotherm models namely Langmuir [40], Freundlich [32], Dubinin-Radushkevich [26] and Temkin [72]. Figure 9 and Table 4 depict the results.

The pertaining equations employed were:

$$\text{Freundlich} : \log\left(q_e\right) = \log k_F + \frac{1}{n}\log C_e$$

$$\text{Langmuir} : \frac{C_e}{q_e} = \frac{a_L}{k_L}C_e + \frac{1}{k_L}; \ \text{Separation factor} : R_L = 1/(1 + a_L C_i)$$

$$\text{Dubinin and Radushkevich} : \ln q_e = \ln q_m - \beta\varepsilon^2; \ \text{where}\ \varepsilon = RT\ln\left(1 + \frac{1}{C_e}\right); \ E = 1/\sqrt{2\beta}$$

$$\text{Temkin} : q_e = B\ln A + B\ln C_e, \ \text{where}\ B = \frac{RT}{b}$$

The Freundlich model explains the multilayer distribution of the adsorbate over the heterogeneous surface of the adsorbent. The slope ranging between 0 and 1 is a measure of surface heterogeneity, becoming more heterogeneous as its value gets closer to zero. As the slope, $1/n$, values range between 0 and 1, the adsorption is favourable [71].
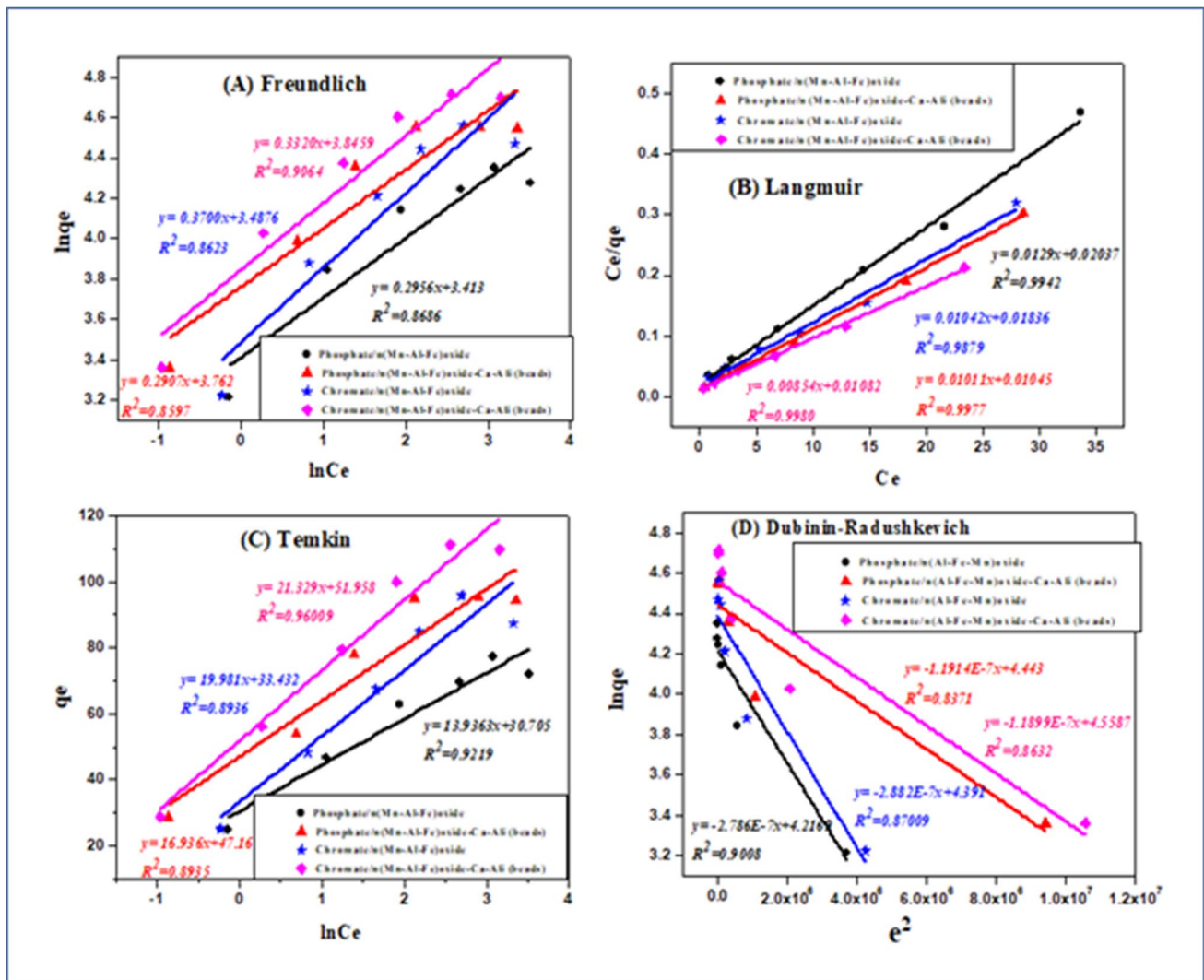

Fig. 9 Adsorption isotherms

Table 4 Evaluated adsorption isotherms parameters

| Adsorbate	Parameters	Freundlich isotherm	Langmuir isotherm	Temkin isotherm	Dubinin-Radushkevich isotherm
Phosphate/n(Mn-Al–Fe)oxide	Slope	0.295	0.0113	13.9	−2.8
	Intercept	3.413	0.204	30.7	4.21
	R^2	0.8686	0.9942	0.9219	0.9008
		$1/n=0.295$	$R_L=0.07$	$B=13.9$	$E=1.34$ kJ/mol
Chromate/n(Mn-Al–Fe)oxide	Slope	0.370	0.0104	19.98	−2.9
	Intercept	3.488	0.0183	33.4	4.39
	R^2	0.8623	0.9879	0.8936	0.8700
		$1/n=0.370$	$R_L=0.08$	19.98	$E=1.3$ kJ/mol
Phosphate/n(Mn-Al–Fe)oxide-Ca-Ali (beads)	Slope	0.291	0.0101	16.9	−1.191
	Intercept	3.76	0.0104	47.2	4.443
	R^2	0.8597	0.9977	0.8935	0.8371
		$1/n=0.291$	$R_L=0.05$	$B=16.9$	$E=2.05$ kJ/mol
Chromate/n(Mn-Al–Fe)oxide-Ca-Ali (beads)	Slope	0.3320	0.0085	21.3	−1.19
	Intercept	3.84	0.01082	51.95	4.664
	R^2	0.9064	0.998	0.960	0.8632
		$1/n=0.332$	$R_L=0.06$	21.3	$E=2.1$ kJ/mol
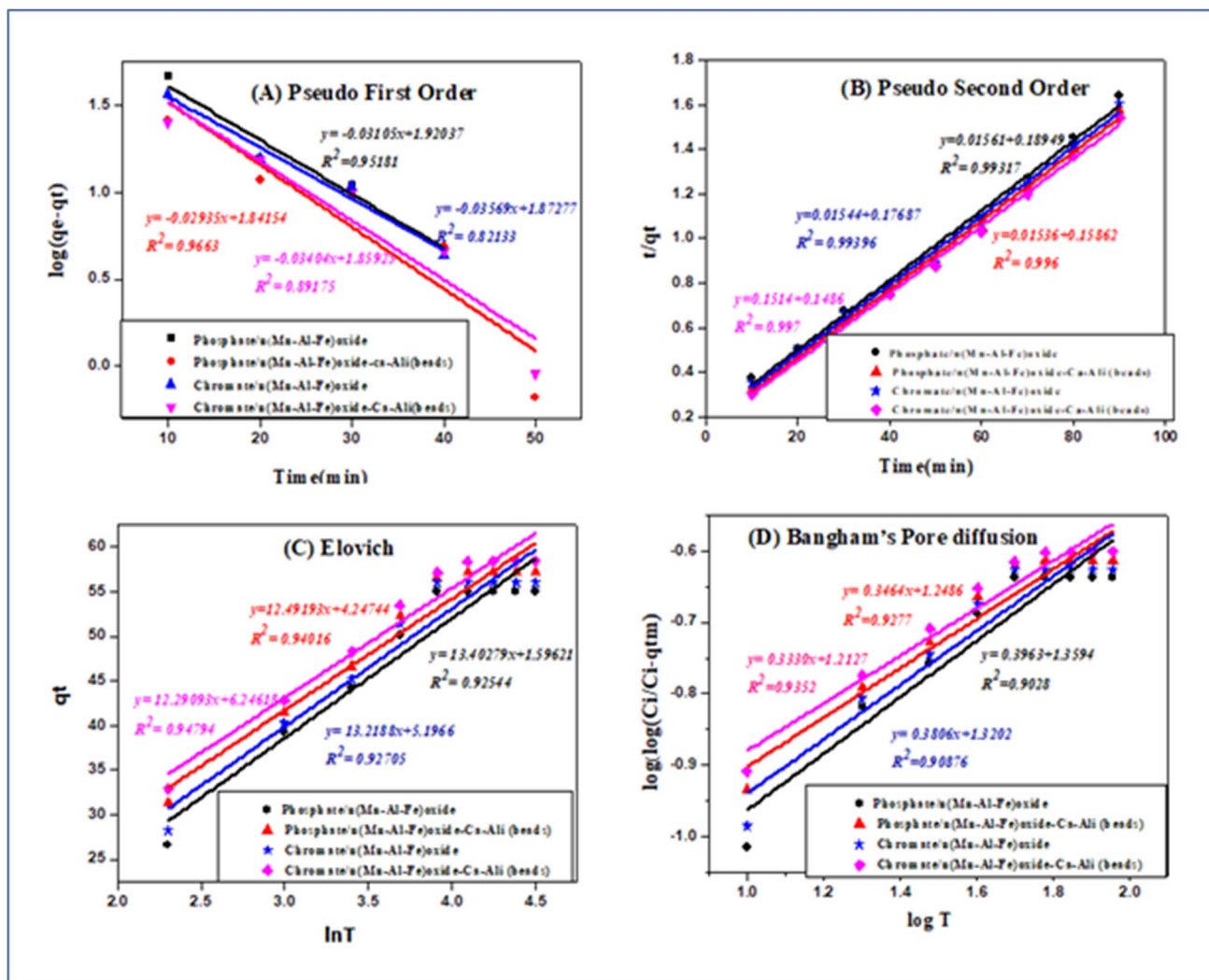
Fig. 10 Kinetics of adsorption

Table 5 Evaluated kinetics parameters of the adsorption process

Models	Parameters	Phosphate/n(Mn-Al–Fe) oxide	Chromate/n(Mn-Al–Fe) oxide	Phosphate/n(Mn-Al–Fe) oxide-Ca-Ali (beads)	Chromate/n(Mn-Al–Fe) oxide-Ca-Ali (beads)
Pseudo first-order model	R^2	0.952	0.821	0.966	0.892
	Intercept	1.920	1.872	1.842	1.859
	Slope	0.031	0.036	0.029	0.034
Pseudo second-order	R^2	0.993	0.993	0.996	0.997
	Intercept	0.189	0.177	0.0158	0.149
	Slope	0.016	0.015	0.0153	0.151
Elovich model	R^2	0.925	0.927	0.940	0.947
	Intercept	1.596	5.196	4.25	6.25
	Slope	13.4	13.22	12.49	12.29
Bangham's pore diffusion	R^2	0.902	0.908	0.927	0.935
	Intercept	1.36	1.320	1.25	1.212
	Slope	0.396	0.380	0.346	0.333

The Temkin model describes the adsorption mechanism on heterogeneous surfaces. This model is based on the assumption that the heat of adsorption of all molecules in the layer will decrease linearly with time mainly due to a decrease in adsorbent-adsorbate interactions during adsorption.

Dubinin-Raduskovich model is applied to express the adsorption mechanism onto both homogeneous and heterogeneous surfaces. The magnitude of energy provides the information about the nature of adsorption reaction. Physisorption is dominated if the D-R mean free energy, E and Temkin heat of sorption (B) are less than 20 kJ/mol [71].

A good fit between the experimental data and the adsorption isotherms was confirmed by correlation coefficient (R^2) values [7, 50]. The model which has a higher R^2 value is best fitted to explain the adsorption process. As is evident from Table 4, R^2 values of the Langmuir model are higher than other models. So, the Langmuir model confirms the monolayer adsorption of chromate and phosphate and homogeneous surface of both the adsorbents, n(Mn-Al–Fe) oxide and n(Mn-Al–Fe) oxide-Ca-Ali (beads). Furthermore, the R_L values, 0.07 for phosphate, 0.08 for chromate with the adsorbent, 'n(Mn-Al–Fe) oxide' and 0.05 for phosphate and 0.06 for chromate with the adsorbent, 'n(Mn-Al–Fe) oxide-Ca-Ali (beads)', also confirm the Langmuir model. As per Hall [34], $0 < R_L < 1$ favours the adsorption. The evaluated R_L values support the favourable nature of the adsorption process. Dubinin-Radushkevich and Temkin equations were used to calculate 'E and B' values.

3.6 Adsorption kinetics

In the present study, the adsorption rates of phosphate and chromate 'onto' the adsorbents, 'n(Mn-Al–Fe) oxide' and 'n(Mn-Al–Fe) oxide-Ca-Ali (beads)', were analysed by four models namely: Pseudo 1st and 2nd order, Bangham's pore
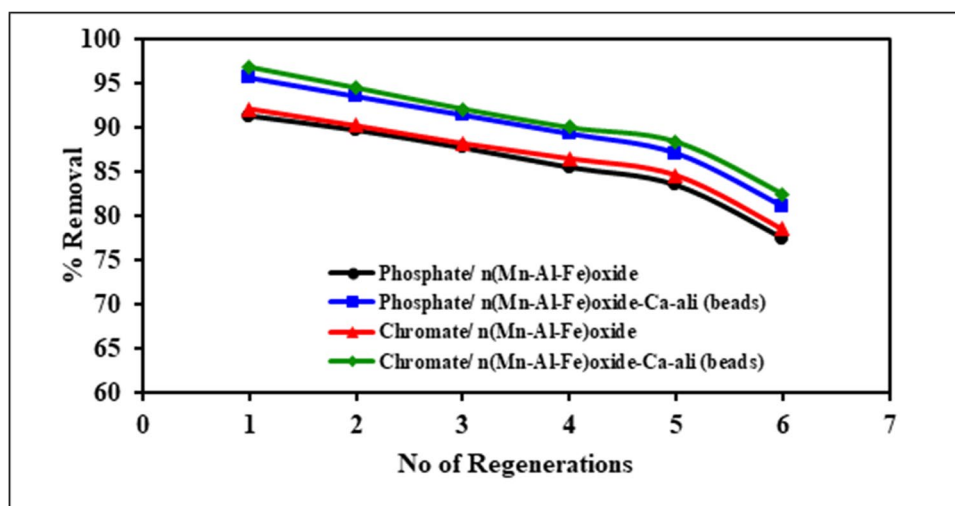
Fig. 11 Number of regenerations vs % removal of phosphate and chromate

Table 6 Applications

A: Nanocomposite[n(Mn-Al–Fe) oxide] as adsorbent: optimum conditions: pH: 7; dosage of composite: 0.13 g/150 mL; contact time: 60 min; rpm: 350; temp.: 30 ± 1 °C)

Samples	Initial conc. of ions, C_i (mg/L)>			Conc. of ions after treatment, C_e (mg/L)		% removal	
	Chromate	Phosphate	Chromate		Phosphate	Chromate	Phosphate
1	2.0	6.8	0		0	100	100
2	2.3	10.5	0		0	100	100
3	3.5	12.5	0		0	100	100
4	4.3	14.5	0		0.5	100	96.5
5	5.6	16.5	0		0.6	100	96.3

B: Beads [n(Mn-Al–Fe) oxide-Ca-Ali] as adsorbent B: optimum conditions: pH: 10; dosage of composite: 0.11 g/150 mL; contact time: 90 min; rpm: 350; temp.: 30 ± 1 °C)

Samples	Initial conc. of ions, C_i (mg/L)		Conc. of ions after treatment, C_e (mg/L)		% removal	
	Chromate	Phosphate	Chromate	Phosphate	Chromate	Phosphate
1	2.0	6.5	0	0	100	100
2	3.0	7.8	0	0	100	100
3	4.5	8.9	0	0	100	100
4	5.5	12.0	0	0	100	100
5	6.0	13.5	0	0	100	100

[*]Mean of six estimations; S.D. ± 0.15

diffusion model and Elovich model as shown in Fig. 10 (Corbett john, [23]; [35, 52, 80]).

The linearized forms of equations used were:

$$\text{Pseudofirstorder}: \log(q_e - q_t) = -\frac{k_1 t}{2.303} + \log(q_e)$$

$$\text{Banghamsequation}: \log.\log\left(\frac{C_i}{C_i - q_t m}\right) = \log\left(\frac{k_o}{2.303V}\right) + \alpha\log(t)$$

$$\text{Pseudosecondorder}: \frac{t}{qt} = \frac{1}{k_2 q^2_e} + \frac{1}{q_e}(t)$$

$$\text{Elovichmodel}: q_t = \frac{1}{\beta}\ln(\alpha\beta) + \frac{1}{\beta}\ln(t)$$

The pseudo first-order model is widely used to describe the adsorption of adsorbate from the liquid phase [13]. The Elovich model is applied for the adsorption of solutes from a liquid solution [67]. Bangham's pore diffusion model is used to describe pore diffusion during the adsorption process [14].

The correlation coefficient (R^2) values reveal the best fitting kinetic model [7]. As seen from Table 5, the R^2 values suggest that the pseudo 2nd-order model better describes the adsorption of 'chromate and phosphate' than the rest models for both the adsorbents.

3.7 Regeneration studies

The reusability of the adsorbents has merits because it reduces the cost of the treatment process. Various eluents such as acids, bases and salts were investigated as eluents in the present regeneration studies [12]. The eluents namely 0.1 N NaOH and 0.1 N HCl were effective to regenerate the adsorbents, n(Mn-Al–Fe) oxide and n(Mn-Al–Fe) oxide-Ca-Ali (beads) respectively.

The results are presented in Fig. 11. As it is seen in the figure, up to sixth regenerations, there is only a marginal efficiency loss and the adsorbents are robust. This is an important merit as the adsorbents can be repetitively used in the treatment of waste water containing phosphate and chromate.

The decline in adsorption with the increase in the number of cycles of regeneration-cum-reuse may be due to loss and/ or non-generation of active sites on the adsorbent's surface. And some of the active sites may be destroyed during the adsorption/desorption process.

Table 7 Comparison of adsorbents

S. no	Sorbent	pH	pollutant	Adsorbent capacity (mg/g)	Reference
1	nZVI @ Fe$_3$O$_4$/graphene	3.0	Chromate	101	(Huang Z. N., et al., [36]
2	(nZVI)/Fe$_3$O$_4$ nanocomposite	8.0	Chromate	29.43	(Lv X., et al., [43]
3	Magnetic MWCNTs	3.0	Chromate	11.4	(Lv X., et al., [44]
4	Fe–Ti nanocomposite	6.8	Phosphate	35.4	(Lu J., et al., [41]
5	La–Zr/Peel	6.2	Phosphate	40.21	(Muhammad A., et al., [53]
6	CNT	5.6	Phosphate	15.4	(Mahdavi S., and Akhzari D. [49]
7	Silver nanoparticles + tea residue active carbon	3.0	Phosphate	13.62	(Trinh V.T., et al., [73]
8	Commercial nanomaterials: Micelle-clay complex	6.0	Chromate	9.43	(Qurie M., et al., [59]
9	Carbon-based nanomaterials: C@La-TiO$_2$	5.0	Chromate	8.2	(Wang J., et al., [77]
10	Carbon-based nanomaterials: Magnetic MWCNTs (MM)	3.0	Chromate	11.4	(Huang Z., et al., [36]
11	ACSCC (AC of Stems of Carissa Carandas plant)	2.0	Chromate;	72.75	(Biftu W.K., et al., [8]
		7.0	Phosphate;	63.40	
12	n(Mn-Al–Fe) oxide	7.0	Phosphate	71.8	Present Work
13	n(Mn-Al–Fe) oxide	7.0	Chromate	87.3	
14	n(Mn-Al–Fe)oxide-Ca-Ali (beads)	10.0	Phosphate	94.3	
15	n(Mn-Al–Fe)oxide-Ca-Ali (beads)	10.0	Chromate	109.8	

3.8 Applications

The real water samples contaminated with chromate and phosphate, collected from leather industrial effluents and polluted lake waters in Guntur District of Andhra Pradesh, India, were analysed for the content of phosphate and chromate. These samples were treated with the new adsorbents developed in this investigation at the optimum conditions established in this work; nanocomposite: at pH: 7; adsorbent dosage: 0.13 g/150 mL; contact time: 60 min; and temperature of 303 K; beads: pH: 10; adsorbent dosage: 0.11 g/150 mL; contact time: 90 min; and temperature of 303 K. The results obtained are presented in Table 6. As seen from the table, the two adsorbents are effective and efficient for the treatment of waste water for the removal of chromate and phosphate from polluted water.

3.9 Comparison with previous works

The established adsorbents, n(Mn-Al–Fe) oxide' and 'n(Mn-Al–Fe) oxide-Ca-Ali (beads)', in the present work were compared with other adsorbents based on nanoparticles in the literature which were used for the removal of phosphate and chromate ions. They were compared with respect to the pH and adsorption capacity of the adsorbents. The results are presented in Table 7. As inferred from the table, the adsorption capacities of the present investigated adsorbent were higher than many other adsorbents in the literature. Hence, the developed adsorbents, 'n(Mn-Al–Fe) oxide' and

'n(Mn-Al–Fe)oxide-Ca-Ali (beads)', were more efficient than hitherto developed adsorbents. Furthermore, the main merits of the present new adsorbents are that chromate and phosphate can be simultaneously removed from polluted waters, if exits.

4 Conclusions

Manganese-based nanoparticles of trinary metal (Mn-Al–Fe) mixed oxides of size 6.19 nm are successfully synthesized via new green methods using 'aloe vera gel' as a capping agent. The precipitant (OH$^-$) is generated slowly by 'urea hydrolysis' in a viscous mother liquor [glycerol:water (20:80)] to prevent supersaturation at local points and facilitate the formation of nanoparticles.

The mixed nanometal oxide and Ca-alginate beads studded with these particles have shown an affinity for 'phosphate and chromate' at pH 7 and 10 respectively. This gives a clue for the simultaneous extraction of phosphate and chromate. So, investigations are carried for the simultaneous removal of 'phosphate and chromate' from water. For simultaneous removal of the said pollutants, the extraction conditions are investigated and optimized. With mixed nanooxides, the optimum conditions are as follows: pH: 7; dosage of sorbent: 0.13 g/150 mL; contact time: 60 min; rpm: 350; and temp.: 30 ± 1 °C; while with beads, the optimum conditions are as follows: pH: 10; dosage of beads: 0.11 g/150 mL; contact time: 90 min; rpm: 350; and temp.:

30 ± 1 °C. The adsorption capacities are 71.8 mg/g for phosphate and 87.3 mg/g for chromate with nanomixed metal oxides as adsorbents. With beads as adsorbents, the adsorption capacities are 94.3 mg/g for phosphate and 109.8 mg/g for chromate. The cumulative sorption nature of nanoparticles and Ca-alginate beads has enhanced the adsorption capacities, and furthermore, the bead structure has prevented the agglomeration of nanoparticles besides facilitating easy filtration. The interferences caused by co-ions are also investigated.

The adsorbents are characterized using various techniques. Endothermic and spontaneous nature of adsorption is confirmed by thermodynamic studies. Pseudo 2nd-order kinetic models and Langmuir isotherms explain well the sorption mechanism. Six cycles of re-generation and re-use of adsorbents are permitted. Real polluted waters are successfully treated adopting the methodologies established in this investigation. The novelty of the present investigation is that manganese-based trinary nanomixed metal (Mn-Al–Fe) oxides and Ca-alginate beads studded with these nanoparticles are green-synthesized and effectively used for the simultaneous removal of 'phosphate and chromate' from polluted water.

Supplementary Information The online version contains supplementary material available at https://doi.org/10.1007/s13399-021-02293-0.

Data availability All data generated or analysed during this study are included in this published article [and its supplementary information files].

Declarations

Conflict of interest The authors declare no competing interests.

References

1. Ai T, Jiang X, Liu Q (2018) Chromium removal from industrial wastewater using Phyllostachys pubescens biomass loaded Cu-S nanospheres. Open Chem 16:842–852
2. Alam JB, Dikshit AK, Bandyopadhayay M (2005) Evaluation of thermodynamic properties of sorption of 2, 4-D and atrazine by tire rubber granules. Sep Purif Technol 42(1):85–90. https://doi.org/10.1016/j.seppur.2004.06.006
3. Apha APHA (1998) Standard methods for the examination of water and waste water. APHA, Washington, DC
4. Arshadi M, Eskandarloo H, Azizi M, Abbaspourrad A, Abdolmaleki MK, Eskandarloo H, Azizi M, Abbaspourrad A (2018) Synthesis of highly monodispersed, stable, and spherical nZVI of 20–30 nm on filter paper for the removal of phosphate from wastewater: batch and column study. ACS Sustain Chem Eng 6:11662–11676. https://doi.org/10.1021/acssuschemeng.8b01885
5. ASTM D4607–94 (2006) Standard test method for determination of iodine number of activated carbon.
6. Badessa T, Shaposhnik V (2016) The electrodialysis of electrolyte solutions of multi-charged cations. J Membr Sci 498:86–93. https://doi.org/10.1016/j.memsci.2015.09.017
7. Badessa TS, Wakuma E, Yimer AM (2020) Bio-sorption for effective removal of chromium (VI) from wastewater using Moringa stenopetala seed powder (MSSP) and banana peel powder (BPP). BMC Chemistry 14(1):1–2. https://doi.org/10.1186/s13065-020-00724-z
8. Biftu WK, Kunta R (2021c) Iron-alginate beads doped with green synthesised 'nano-CeO$_2$-ZrO$_2$'as an effective adsorbent for removal of highly toxic arsenic-ions from polluted waterInt J Environ Anal Chem 1–19https://doi.org/10.1080/03067319.2021.1875452
9. Biftu WK, Mekala S, Ravindhranath K (2020) De-fluoridation of polluted water using aluminium alginate beads doped with green synthesized 'nano SiO$_2$+ nano CeO$_2$-ZrO$_2$', as an effective adsorbent. Chemistry Select 5(47):15061–15074. https://doi.org/10.1002/slct.202003744
10. Biftu WK, Ravindhranath K (2020) Synthesis of nanoZrO$_2$ via simple new green routes and its effective application as adsorbent in phosphate remediation of water with or without immobilization in Al-alginate beads. Water Sci Technol 81(12):2617–2633. https://doi.org/10.2166/wst.2020.318
11. Biftu WK, Ravindhranath K (2021) Calcium alginate beads doped with nano-ZrO$_2$ and activated carbon of Annona reticulata plant as an effective adsorbent for water remediation of chromium(VI). Asian J Chem 33(2):281–290. https://doi.org/10.14233/ajchem.2021.22953
12. Biftu WK, Ravindhranath K, Ramamoorty M (2020) New research trends in the processing and applications of iron-based nanoparticles as adsorbents in water remediation methods. Nanotechnol Environ Eng 5:1–12. https://doi.org/10.1007/s41204-020-00076-y
13. Biftu WK, Suneetha M, Ravindhranath K (2021) Sequential adsorptive removal of phosphate, nitrate and chromate from polluted water using active carbon derived from stems of Carissa carandas plant. Water Pract Technol, IWA Publishing 16(1):117–134. https://doi.org/10.2166/wpt.2020.102
14. Biftu WK, Suneetha M, Ravindhranath K (2021b) Zirconium-alginate beads doped with H$_2$SO$_4$-activated carbon derived from leaves of Magnoliaceae plant as an effective adsorbent for the removal of chromate. Biomass Convers Biorefin 1-16https://doi.org/10.1007/s13399-021-01568-w
15. BIS (Bureau of Indian Standards) (1989) Activated carbon, powdered and granular-methods of sampling and its tests BIS New Delhi 877.
16. Biswas K, Gupta K, Goswami A (2010) Ghosh UC Fluoride removal efficiency from aqueous solution by synthetic iron(III)–aluminum(III)–chromium(III) ternary mixed oxide. Desalination 255(1–3):44–51. https://doi.org/10.1016/j.desal.2010.01.019
17. Bouamra F, Drouiche N, Abdi N, Grib H, Mameri N, Lounici H (2018) Removal of phosphate from wastewater by adsorption on marble waste: effect of process parameters and kinetic modeling. Int J Environ Res 12:13–27. https://doi.org/10.1007/s41742-018-0065-3
18. Brunauer S, Emmett PH, Teller E (1938) Adsorption of gases in multimolecular layers. J Am Chem Soc 60(2):309–319. https://doi.org/10.1021/ja01269a023
19. Bunce JT, Ndam E, Ofiteru ID, Moore A, Graham DW (2018) A review of phosphorus removal technologies and their applicability to small-scale domestic wastewater treatment systems. Front Environ Sci 6:8. https://doi.org/10.3389/fenvs.2018.00008
20. Bureau of Indian Standards (1991) IS: 10500.
21. Cai W, Fu F, Zhu L, Tang B (2019) Simultaneous removal of chromium(VI) and phosphate from water using easily separable magnetite/pyrite nanocomposite. J Alloy Compd 803:118–125. https://doi.org/10.1016/j.jallcom.2019.06.285
22. Chen D, Xiao X, Yang K (2016) Removal of phosphate and hexavalent chromium from aqueous solutions by engineered waste eggshell. RSC Adv. https://doi.org/10.1039/C6RA05034D

23. Corbett JF (1972) Pseudo first-order kinetics. J Chem Educ 49:663. https://doi.org/10.1016/j.jece.2018.01.014

24. Dorofeev GA, Streletskii AN, Povstugar IV, Protasov AV, Elsukov EP (2012) Determination of nanoparticle sizes by X-ray diffraction. Colloid J 74(6):675–685. https://doi.org/10.1134/S1061933X12060051

25. Duan H, Zhang L, Wang Y, Liu Y, Wang Y (2021) Phosphate removal from aqueous solution by Fe-La binary (hydr)oxides: a study of batch experiments and mechanisms. Environ Sci Pollut Res. https://doi.org/10.1007/s11356-021-15127-3

26. Dubinin MM, Radushkevich LV (1947) The equation of the characteristic curve of the activated charcoal. Proc Acad Sci Phys Chem Sect USSR 55:331–333

27. El-Hendawy ANA, Samra SE, Girgis BS (2001) Adsorption characteristics of activated carbons obtained from corncobs. Colloids Surf, A 180(3):209–221. https://doi.org/10.1016/S0927-7757(00)00682-8

28. Eljamal O, Khalil AME, Matsunaga N (2017) Experimental and modeling column study of phosphorus removal by permeable reactive materials. Int J Environ Agric Res 3(1):62–70

29. Eljamal O, Okawauchi J, Hiramatsu K (2014) Product rich in phosphorus produced from phosphorus-contaminated water. Adv Mater Res 894:261–265

30. Eljamal R, Eljamal O, Maamoun I, Yilmaz G, Sugihara Y (2020) Enhancing the characteristics and reactivity of nZVI: polymer's effect and mechanisms. J Mol Liq 315:113714. https://doi.org/10.1016/j.molliq.2020.113714

31. Fan C, Zhang Y (2018) Adsorption isotherms, kinetics and thermodynamics of nitrate and phosphate in binary systems on a novel adsorbent derived from corn stalks. J Geochem Explor 188:95–100. https://doi.org/10.1016/j.gexplo.2018.01.020

32. Freundlich HMF (1906) Over the adsorption in solution. J Phys Chem 57(385471):1100–1107

33. George WK, Eren Y, Ayd S, Emik S, Tuba A, Osra F, Wasswa J (2019) A facile polymerisation of magnetic coal to enhanced phosphate removal from solution. J Environ Manag 247:356–362. https://doi.org/10.1016/j.jenvman.2019.06.088

34. Hall KR, Eagleton LC, Acrivos A, Vermeulen T (1966) Pore-and solid-diffusion kinetics in fixed-bed adsorption under constant-pattern conditions. Ind Eng Chem Fundam 5(2):212–223. https://doi.org/10.1021/i160018a011

35. Ho YS, McKay G (1999) Pseudo-second order model for sorption processes. Process Biochem 34(5):451–465. https://doi.org/10.1007/s11356-019-05050-z

36. Huang Z, Wang X, Yang D (2015) Adsorption of Cr (VI) in wastewater using magnetic multi-wall carbon nanotube. Water Sci Eng 8(3):226–232. https://doi.org/10.1016/j.wse.2015.01.009

37. Jiang J, Yuan M, Xu R, Bish DL (2015) Mobilization of phosphate in variable-charge soils amended with biochars derived from crop straws. Soil Tillage Res 146:139–147. https://doi.org/10.1016/j.still.2014.10.009

38. Jin T, Yuan W, Xue Y, Wei H, Zhang C, Li K (2017) Co-modified MCM-41 as an effective adsorbent for levofloxacin removal from aqueous solution: optimization of process parameters, isotherm, and thermodynamic studies. Environ Sci Pollut Res 24(6):5238–5248. https://doi.org/10.1007/s11356-016-8262-0

39. Kahani SA, Jafari M (2009) A new method for preparation of magnetite from iron oxyhydroxide or iron oxide and ferrous salt in aqueous solution. J Magn Magn Mater 321(13):1951–1954. https://doi.org/10.1016/j.jmmm.2008.12.026

40. Langmuir I (1918) The adsorption of gases on plane surfaces of glass, mica and platinu. J Am Chem Soc 40(9):1361–1403. https://doi.org/10.1021/ja02242a004

41. Lu J, Liu D, Hao J, Zhang G, Lu B (2005) Phosphate removal from aqueous solutions by a nano-structured Fe–Ti bimetal oxide sorbent. Chem Eng Res Des 93:652–661. https://doi.org/10.1016/j.cherd.2014.05.001

42. Lu J, Liu H, Liu R, Zhao X (2013) Adsorptive removal of phosphate by a nanostructured Fe–Al–Mn tri metal oxide adsorbent. Powder Technol 233:146–154. https://doi.org/10.1016/j.powtec.2012.08.024

43. Lv X, Jiang XXue G, Wu D, Sheng T, Zhou H, Xu X (2014) Journal of colloid and interface science 417–51.

44. Lv X, Xue G, Jiang J, Tang X Xu (2012) Journal of colloid and interface science 369–460.

45. Maamoun I, Eljamal O, Eljamal R, Falyouna O, Sugihara Y (2020c) Promoting aqueous and transport characteristics of highly reactive nanoscale zero valent iron via different layered hydroxide coatings. Appl Surf Sci 145018https://doi.org/10.1016/j.apsusc.2019.145018

46. Maamoun I, Eljamal O, Falyouna O, Eljamal R, Sugihara Y (2020) multi-objective optimization of permeable reactive barrier design for Cr (VI) removal from groundwater. Ecotoxicol Environ Saf 200:110773. https://doi.org/10.1016/j.ecoenv.2020.110773

47. Maamoun I, Eljamal O, Falyouna O, Eljamal R, Sugihara Y (2020) Stimulating effect of magnesium hydroxide on aqueous characteristics of iron nanocomposites. Water Sci Technol. https://doi.org/10.2166/wst.2020.027

48. Maamoun I, Falyouna O, Eljamal R, Bensaida K, Eljamal O (2021) Optimization modeling of nFe0/Cu-PRB design for Cr(VI) removal from groundwater. International J Environ Sci Dev 12:(5). https://doi.org/10.18178/ijesd.2021.12.5.1330

49. Mahdavi S, Akhzari D (2016) The removal of phosphate from aqueous solutions using two nano-structures: copper oxide and carbon tubes. Clean Technol Environ Policy 18(3):817–827. https://doi.org/10.1007/s10098-015-1058-y

50. Mekonnen DT, Alemayehu E, Lennartz B (2021) Adsorptive removal of phosphate from aqueous solutions using low-cost volcanic rocks: kinetics and equilibrium approaches. Materials 14:1312. https://doi.org/10.3390/ma14051312

51. Mohammad A, Inamuddin Hussain S (2014) Poly (3,4-ethylenedioxythiophene): polystyrene sulfonate (PEDOT: PSS) Zr(IV) phosphate composite cation exchanger: sol-gel synthesis and physicochemical characterization. Ionics 21:1063–1071. https://doi.org/10.1007/s11581-014-1247-4

52. Mohan GK, Babu AN, Kalpana K, Ravindhranath K (2019) Removal of chromate (VI) from water using adsorbent derived from spent coffee grounds. Int J Environ Sci Technol 16(1):101–112. https://doi.org/10.1007/s13762-017-1593-7

53. Muhammad A, Xing X, Baoyu G, Qinyan Y, Shang Y, Rizwan K, Muhamma AI (2020) Adsorptive removal of phosphate by the bimetallic hydroxide nanocomposites embedded in pomegranate peel. J Environ Sci 91:189–198. https://doi.org/10.1016/j.jes.2020.02.005

54. Onyango MS, Kojima Y, Aoyi O, Bernardo EC, Matsuda H (2004) Adsorption equilibrium modeling and solution chemistry dependence of fluoride removal from water by trivalent-cation-exchanged zeolite F-9. J Colloid Interface Sci 279(2):341–350. https://doi.org/10.1016/j.jcis.2004.06.038

55. Owlad M, Aroua MK, Wan Daud WA, Baroutian S (2008) Removal of hexavalent chromium-contaminated water and wastewater: a review. Water Air Soil Pollut. https://doi.org/10.1007/s11270-008-9893-7

56. Panda H, Tiadi N, Mohanty M, Mohanty CR (2017) Studies on adsorption behavior of an industrial waste for removal of chromium from aqueous solution. S Afr J Chem Eng 23:132–138. https://doi.org/10.1016/j.sajce.2017.05.002

57. Qin Q, Wang Q, Fu D, Ma J (2011) An efficient approach for Pb(II) and Cd(II) removal using manganese dioxide formed in situ. Chem Eng J 172(1):68–74. https://doi.org/10.1016/j.cej.2011.05.066

58. Qiu H, Liang C, Yu J, Zhang Q, Song M, Chen F (2017) Preferable phosphate sequestration by nano-La (III) (Hydr) oxides modified wheat straw with excellent properties in regeneration. Chem Eng J 315:345–354. https://doi.org/10.1016/j.cej.2017.01.043

59. Qurie M, Khamis M, Manassra A, Ibrahim A, Shlomo N, Scrano L, Bufo SA, Rafik K (2013) Removal of Cr(VI) from aqueous environments using micelle-clay adsorption. Scientific World Journal. https://doi.org/10.1155/2013/942703

60 Ravindhranath K, Ramamoorty M (2017) Nickel based nano particles as adsorbents in water purification methods-a review. Oriental J Chem 33(4):1603. https://doi.org/10.13005/ojc/330403

61. Rezak N, Bahmani A, Bettahar N (2021) Adsorptive removal of P(V) and Cr (VI) by calcined Zn-Al-Fe ternary LDHs. Water Sci Technol 83(10):2504–2517. https://doi.org/10.2166/wst.2021.123

62. Ruzhitskaya O, Gogina E (2017) Methods for removing of phosphates from wastewater. MATEC Web of Conferences 106:07006. https://doi.org/10.1051/matecconf/201710607006

63. Salah Abde WM, Abdel Monem AS, Mohamed A, Mohamed MA (2013) Adsorption Studies on the removal of hexavalent chromium contaminated wastewater using activated carbon and bentonite. Asian J Chem 25(15):8245–8252

64. Sereshti H, ZamiriAfsharian E, EsmaeiliBidhendi M, RashidiNodeh H, AfzalKamboh M, Yilmaz M (2020) Removal of phosphate and nitrate ions aqueous using strontium magnetic graphene oxide nanocomposite: isotherms, kinetics, and thermodynamics studies. Environ Prog Sustainable Energy 39(2):13332. https://doi.org/10.1002/ep.13332

65. Shokrollahi M et al (2019) Application of ZnO nanostructures in ceramic and polymeric membranes for water and wastewater technologies. Chem Eng J 391:123475. https://doi.org/10.1016/j.cej.2019.123475

66. Shokrollahi M, Rezakazemi M, Younas M (2020) Producing water from saline streams using membrane distillation: modeling and optimization using CFD and design expert. Int J Energy Res 44(11):8841–8853. https://doi.org/10.1002/er.5578

67. Sneha Latha P, Biftu WK, Suneetha M, Ravindhranath K (2021) De-fluoridation studies: using Lanthanum-alginate-beads impregnated with green synthesized nSiO₂ and active carbon of Terminalia ivorensis plant as an effective adsorbent. Int J Environ Sci Technol. https://doi.org/10.1007/s13762-021-03575-w

68. Stella C, Soundararajan N, Ramachandran K (2014) Structural, optical, dielectric and magnetic properties of $Mn_{1-x}Co_xO_2$ nanowires. Superlattices Microstruct 71:203–210. https://doi.org/10.1016/j.spmi.2014.03.044

69. Suneetha M, Ravindhranath K (2015) Adsorption of nitrite ions onto the bio-sorbents derived from Azadirachta indica plant. Asian J Wate Environ Pollut 14(2):71–79

70. Suneetha M, Ravindhranath K (2018) Removal of nitrites from waste waters using adsorbents derived from Phyllanthus neruri plant. Indian J Chem Technol 25(4):345–352

71. Suneetha M, Syama S, Rabindranath K (2015) De-fluoridation of waters using low-cost HNO₃ activated carbon derived from stems of Senna occidentalis plant. Int J Environ Technol Manage 18(5/6):420–447. https://doi.org/10.1504/IJETM.2015.073079

72. Temkin MJ, Pyzhev V (1940) Recent modifications to Langmuir isotherms. Acta Physiochim USSR 12:217–222

73. Trinh VT, Nguyen TMP, Hoang HT, Van LP, Nguyen TV, Ha LT, Xuan HV, Pham TT, Nguyen TN, Quang NV, Nguyen (2020) Phosphate adsorption by silver nanoparticles-loaded activated carbon derived from tea residue. Sci Rep 10(1). https://doi.org/10.1038/s41598-020-60542-0

74. Trivedy R K (1995) Pollution management in industries, Environmental Publications. 2nd Ed Karad India.

75. US Department of Health and Human Services Profile for Chromate (1991) Public Health Service Agency for toxic substances and diseases. Washington DC.

76. Wang H, Xu X, Ren Z, Gao B (2016) Removal of phosphate and chromium (VI) from liquids by an amine-crosslinked nano-Fe₃O₄biosorbent derived from corn straw. RSC Adv 6:47237–47248. https://doi.org/10.1039/C6RA06801D

77. Wang J, Liang Y, Jin Q, Hou J, Liu B, Li X, Chen X, Hayat W, Ahmed T, Wang A (2017) Simultaneous removal of graphene oxide and chromium(VI) on the rare earth doped titanium dioxide coated carbon sphere composites. ACS Sustainable Chem Eng 56:5550–5561. https://doi.org/10.1021/acssuschemeng.7b00957

78. Wang Y, Xie X, Chen X, Huang C, Yang S (2020) Biochar-loaded Ce3+-enriched ultra-ne ceria nanoparticles for phosphate adsorption. J Hazard Mater 396:122626

79. Wang Z, Fang W, Xing M, Wu D (2017) A bench-scale study on the removal and recovery of phosphate by hydrous zirconia coated magnetite nanoparticles. J Magn Magn Mater 424:213–220. https://doi.org/10.1016/j.jmmm.2016.10.067

80. Wu FC, Tseng RL, Juang RS (2009) Characteristics of Elovich equation used for the analysis of adsorption kinetics in dye-chitosan systems. Chem Eng J 150(2–3):366–373. https://doi.org/10.1016/j.cej.2009.01.014

81. Yadesa W, Taddesse AM, Kibret K, Dechassa N (2018) Synthesis and characterization of fe-al-mn nanocomposite sorbent for phosphate sorption-desorption study. Bull Chem Soc Ethiop 32(3):421–436. https://doi.org/10.4314/bcse.v32i3.2

82. Yao DZR, Sun C, Zheng Y, Cheng Liu C (2021) Effluents by recoverable La(OH)₃/foamed nickel adsorbent. ACS Omega 6:5399–5407. https://doi.org/10.1021/acsomega.0c05489

83. Yujin T, Jonas W, Harald K, Martin W, Peter S, Kramer RC (2015) Optically probing Al—O and O—H vibrations to characterize water adsorption and surface reconstruction on α-alumina: an experimental and theoretical study. The J of Chemical Physics 142(054704):1–12. https://doi.org/10.1063/1.4906346